CANCER

MicroRNAs Differentially Regulated by Akt Isoforms Control EMT and Stem Cell Renewal in Cancer Cells

Dimitrios Iliopoulos,[1]* Christos Polytarchou,[2]* Maria Hatziapostolou,[2] Filippos Kottakis,[2] Ioanna G. Maroulakou,[2] Kevin Struhl,[1] Philip N. Tsichlis[2]†

(Published 13 October 2009; Volume 2 Issue 92 ra62)

Although Akt is known to play a role in human cancer, the relative contribution of its three isoforms to oncogenesis remains to be determined. We expressed each isoform individually in an *Akt1*$^{-/-}$/*Akt2*$^{-/-}$/*Akt3*$^{-/-}$ cell line. MicroRNA profiling of growth factor–stimulated cells revealed unique microRNA signatures for cells with each isoform. Among the differentially regulated microRNAs, the abundance of the miR-200 family was decreased in cells bearing Akt2. Knockdown of Akt1 in transforming growth factor–β (TGFβ)–treated MCF10A cells also decreased the abundance of miR-200; however, knockdown of Akt2, or of both Akt1 and Akt2, did not. Furthermore, Akt1 knockdown in MCF10A cells promoted TGFβ-induced epithelial-mesenchymal transition (EMT) and a stem cell–like phenotype. Carcinomas developing in MMTV-cErbB2/*Akt1*$^{-/-}$ mice showed increased invasiveness because of miR-200 down-regulation. Finally, the ratio of Akt1 to Akt2 and the abundance of miR-200 and of the messenger RNA encoding E-cadherin in a set of primary and metastatic human breast cancers were consistent with the hypothesis that in many cases, breast cancer metastasis may be under the control of the Akt–miR-200–E-cadherin axis. We conclude that induction of EMT is controlled by microRNAs whose abundance depends on the balance between Akt1 and Akt2 rather than on the overall activity of Akt.

INTRODUCTION

Akt is a serine-threonine protein kinase that is activated by phosphorylation at two sites (Thr^{308} and Ser^{473}) through a phosphatidylinositol 3-kinase (PI3K)–dependent process. Specifically, growth factor signals and other stimuli that activate PI3K promote the accumulation of D3-phosphorylated phosphoinositides at the plasma membrane. The interaction of these phosphoinositides with the pleckstrin homology (PH) domain of Akt promotes the translocation of the kinase to the plasma membrane, where it undergoes phosphorylation by PI3K-dependent kinase–1 (PDK1) at Thr^{308} and by mTOR (mammalian target of rapamycin) complex–2 (TORC2) at Ser^{473} (*1*–*3*).

Ample evidence links Akt with the induction and progression of human cancer (*4*). However, there are three Akt isoforms and information regarding their specific oncogenic activities is limited. The Akt1 and Akt2 isoforms appear to play different roles in mammary adenocarcinomas induced in mice by transgenes encoding the oncoproteins polyoma middle T and ErbB2 (also known as Neu), both of which activate the PI3K-Akt pathway. Indeed, ablation of Akt1 inhibits—whereas ablation of Akt2 accelerates—tumor induction and growth by both polyoma middle T and ErbB2 (*5*, *6*). However, the tumors developing in the Akt1 knockout mice are more invasive than the tumors developing in Akt2 knockout and wild-type mice (*5*), suggesting that ablation of Akt1 may also enhance tumor invasiveness, a process separate from and independent of tumor induction and growth (*7*). These findings were consistent with observations showing that Akt1 knockdown promotes migration and invasiveness of human mammary epithelial cells in culture (*8*–*10*), perhaps by promoting epithelial-mesenchymal transition (EMT), a process that plays important roles in both development and oncogenesis. During EMT, epithelial cells acquire a mesenchymal phenotype characterized by the loss of intercellular junctions and increased cell mi-

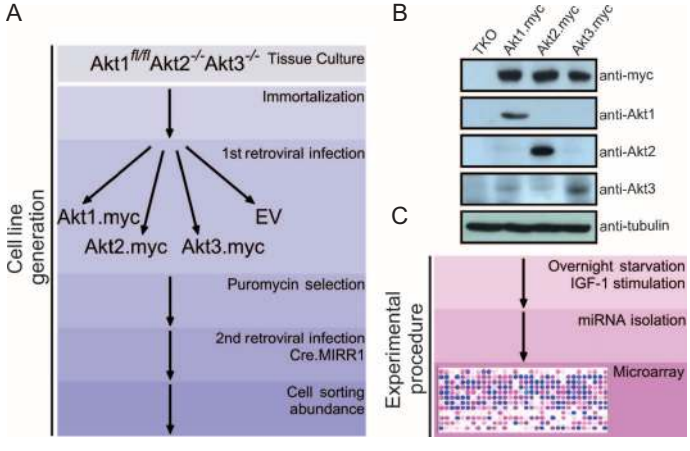

Fig. 1. Strategy for generating lung fibroblasts based on abundance of different Akt isoforms and for the identification of IGF-1–induced microRNAs. (**A**) Cells were transduced to express different Akt isoforms. (**B**) Western blots of cell lysates were probed with antibody directed against the myc tag or with antibodies directed against Akt1, Akt2, or Akt3. Tubulin was used as a loading control. (**C**) Cell lysates harvested before and after IGF-1 treatment were screened with a 365 microRNA array.

[1]Department of Biological Chemistry and Molecular Pharmacology, Harvard Medical School, Boston, MA 02115, USA. [2]Molecular Oncology Research Institute, Tufts Medical Center, Boston, MA 02111, USA.
*These authors contributed equally to this work.
†To whom correspondence should be addressed. E-mail: ptsichlis@tuftsmedicalcenter.org

gration. On the molecular level, cells undergoing EMT decrease the abundance of epithelial cell–specific proteins, such as E-cadherin, and increase the abundance of mesenchymal cell–specific proteins, such as vimentin. The developmental switch characteristic of EMT renders tumor cells undergoing this process more invasive and metastatic. Thus, inhibition of individual Akt isoforms may have both desirable and undesirable effects during oncogenesis. We therefore wished to identify and characterize the downstream targets of Akt isoforms, which may discriminate the beneficial from the detrimental effects of isoform-specific Akt inhibition.

MicroRNAs are a class of molecules that regulate gene expression by various mechanisms and play important roles in oncogenesis (*11*, *12*). Like conventional oncogenes and tumor suppressor genes, microRNAs may either promote or inhibit oncogenesis. Also, like conventional cancer genes, their expression is selectively increased or decreased in various human and animal tumors. The selective deregulation of microRNA gene

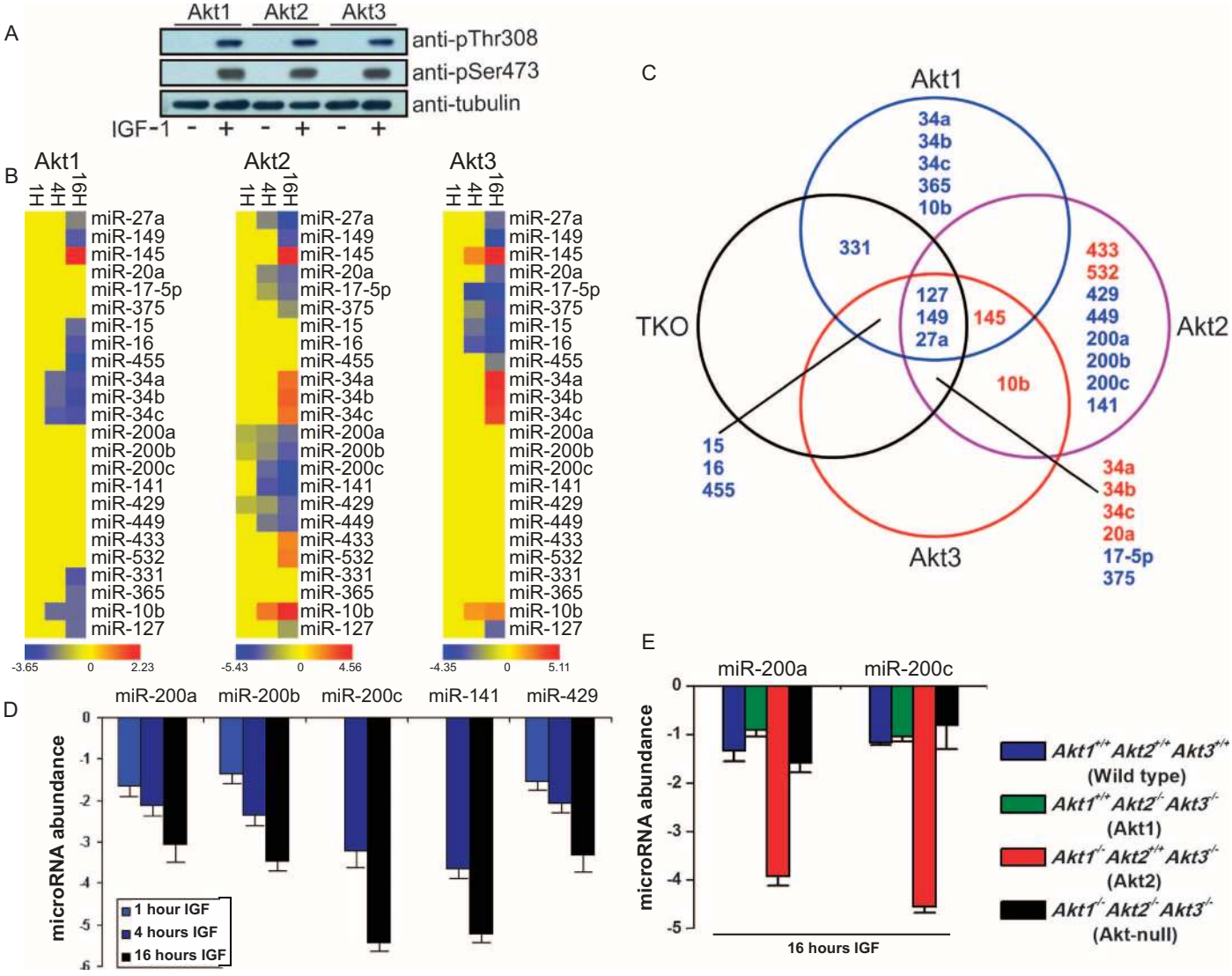

Fig. 2. Akt isoforms have different microRNA gene signatures. (**A**) IGF-1 treatment induces the phosphorylation of all Akt isoforms at Ser^{473} and Thr^{308} (in Akt1 or the equivalent sites in Akt2 and Akt3) in murine lung fibroblasts engineered to express Akt1, Akt2, or Akt3. After overnight serum starvation, cells were treated with IGF-1 (50 ng/ml) for 10 min and cell lysates were analyzed by Western blot. Tubulin was used as a loading control. (**B**) Heat map of differentially expressed microRNAs in untreated and IGF-1–treated (1, 4, and 16 hours) fibroblasts carrying individual Akt isoforms. Red indicates up-regulation, and blue indicates down-regulation. (**C**) Overlap between the microRNA signatures of IGF-1–treated (16 hours) Akt1, Akt2, Akt3, and TKO fibroblasts. (**D**) The abundance of miR-200 family members was measured by real-time RT-PCR 1, 4, and 16 hours after IGF-1 treatment. MicroRNA abundance before the IGF-1 treatment was set to 0. MiR-200 family members were down-regulated after IGF-1 treatment only in Akt2-expressing fibroblasts. (**E**) Down-regulation of miR-200a and miR-200c in Akt2-expressing MEFs. The expression of miR-200 family members was measured at 16 hours after IGF-1 treatment by real-time RT-PCR. The experiments were performed in triplicate and data are presented as mean ± SD.

expression may be due to deletions, amplifications, or mutations targeting the microRNAs themselves or their regulatory sequences, as well as to dysregulation of transcription factors and epigenetic regulators targeting the genes encoding them (*13*). Understanding the regulation and functional activities of individual microRNA families in cancer and other human diseases could thus lead to new opportunities for therapeutic intervention.

Here, we describe a set of microRNAs that are differentially regulated by the three Akt isoforms in cells stimulated with insulin-like growth factor 1 (IGF-1), a treatment that activates Akt. In addition, we show that a decrease in the abundance of the miR-200 microRNA family in cells in which the ratio of Akt1 to Akt2 was decreased promotes EMT and the acquisition of a stem cell–like phenotype in cultured cells, as well as in mouse and human tumors. Down-regulation of the miR-200 microRNA family in these cells appears to depend not on Akt activity per se, but on the balance between Akt1 and Akt2.

RESULTS

Akt isoforms have different microRNA gene signatures

Lung fibroblast and kidney epithelial cells from $Akt1^{fl/fl}/Akt2^{-/-}/Akt3^{-/-}$ mice were immortalized as described in Materials and Methods. The immortalized lung fibroblasts were transduced with myc-tagged Akt1, Akt2, or Akt3 retroviral constructs or with the empty retroviral vector. Knocking out the floxed Akt1 allele in these cells with Cre recombinase gave rise to cell lines that expressed only one of the three Akt isoforms. Knocking out the floxed Akt1 in the vector-transduced cells gave rise to Akt-null cells, which survived for about a week, but failed to proliferate. The abundance of mycAkt1, mycAkt2, and mycAkt3 in cell lines engineered to express a single Akt isoform was similar (Fig. 1). Moreover, the abundance of mycAkt1 in these cell lines was about two times higher and the abundance of mycAkt3 three times higher than the abundance of endogenous Akt1 and Akt3, respectively, in primary lung fibroblasts. How-

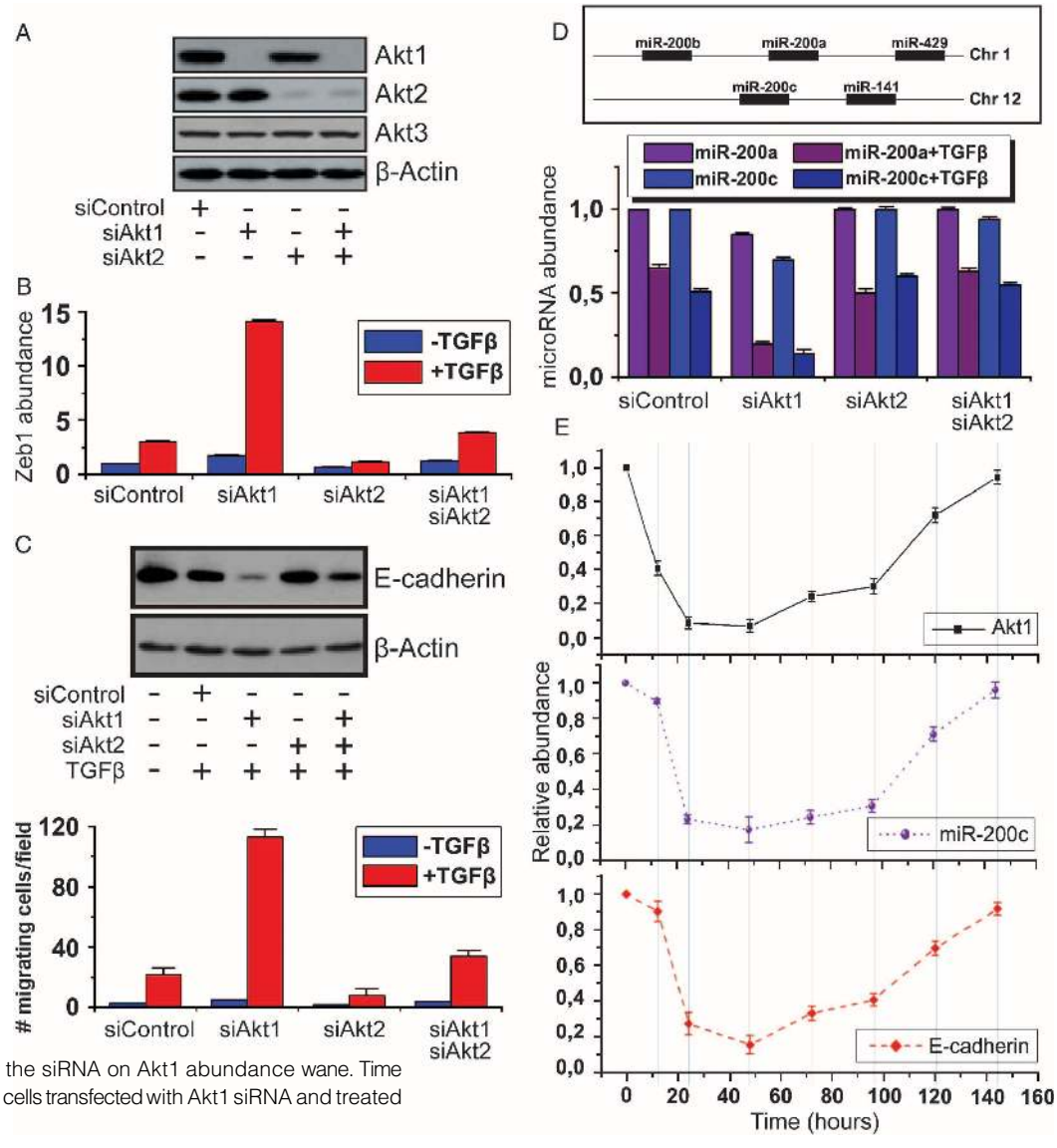

Fig. 3. Knockdown of Akt1 promotes EMT by decreasing abundance of the miR-200 microRNA family. (**A**) Knockdown of Akt1 and Akt2 in MCF10A cells. Western blots of cell lysates after transfection of Akt1, Akt2, or Akt1 and Akt2 siRNAs probed with the indicated antibodies. (**B**) TGFβ synergizes with Akt1 knockdown to increase Zeb1 abundance. Zeb1 abundance measured by real-time PCR in cells transfected with the indicated siRNAs and treated with TGFβ. (**C**) Akt1 knockdown promotes EMT. (Upper panel) The knockdown synergizes with TGFβ to decrease E-cadherin abundance. Lysates of cells transfected with the indicated siRNAs and treated with TGFβ, probed with antibodies against E-cadherin and β-actin. (Lower panel) The knockdown synergizes with TGFβ to stimulate cell migration. Cell migration of TGFβ-stimulated cells transfected with the indicated siRNAs. (**D**) (Upper panel) Chromosomal map of the miR-200 microRNA family. (Lower panel) The knockdown synergizes with TGFβ to decrease abundance of miR-200a and miR-200c. MicroRNA abundance was measured by real-time PCR. (**E**) The abundance of miR-200c and the mRNA encoding E-cadherin in cells transfected with Akt1 siRNA returned to pre-transfection values as the effect of the siRNA on Akt1 abundance wane. Time course analysis by real-time RT-PCR in cells transfected with Akt1 siRNA and treated with TGFβ.

ever, the abundance of the individual Akt isoforms in these cell lines never exceeded that of total Akt in the primary cells (fig. S1).

To determine the role of the three Akt isoforms on the abundance of microRNAs, we stimulated Akt-null cells and cells expressing a single Akt isoform with IGF-1, which activates the Akt kinase. Probing whole-cell lysates harvested before and after IGF-1 stimulation with phosphospecific antibodies recognizing activated Akt phosphorylated at Thr^{308} and Ser^{473} confirmed that IGF-1 activated all three Akt isoforms (Fig. 2A). After confirmation of the activation of Akt, we screened cell lysates harvested before and after IGF-1 treatment with a 365 microRNA array. Based on this analysis, we found no differences in microRNA abundance between cells carrying different Akt isoforms under basal conditions; however, IGF-1 treatment elicited marked differences in the microRNA signature of the different groups (Fig. 2B). In cells with Akt1, IGF-1 increased or decreased the abundance of 1 and 12 microRNAs, respectively, whereas in cells with Akt2, it increased or decreased the abundance of 7 and 12 microRNAs, respectively; finally, in cells with Akt3, IGF-1 increased the abundance of 5 and decreased the abundance of 9 microRNAs (Fig. 2B). The abundance of some microRNAs (miR-27a, miR-149, and miR-145) changed in the same direction, but differed quantitatively between IGF-1–treated cells expressing different Akt isoforms, whereas the abundance of other microRNAs changed in the opposite direction in these cells (Fig. 2C, fig. S2, and tables S1 and S2). MicroRNAs whose regulation by different Akt isoforms was qualitatively different included the members of the miR-200 microRNA family (miR-200a, miR-200b, miR-200c, miR-141, and miR-429), whose abundance was decreased after IGF-1 treatment only in Akt2-expressing cells (Fig. 2, B and C). These microRNAs had been previously clustered in a family because they are coordinately regulated and they share seed sequences and targets (*14*, *15*). We confirmed the differential regulation of the miR-200 microRNA family by the three Akt isoforms by real-time reverse transcription polymerase chain reaction (RT-PCR) (Fig. 2D and fig. S3). The Akt2-specific decrease in miR-200 microRNA family abundance was also apparent in IGF-1–treated primary mouse embryonic fibroblasts (Fig. 2E) and in IGF-1–treated immortalized lung fibroblasts transduced with MigR1-GFP (green fluorescent protein) constructs of Akt1, Akt2, or Akt3 (fig. S4). A decrease in the abundance of miR-200c and miR-200a was also observed in cells transduced with constitutively active MyrAkt1, MyrAkt2, or MyrAkt3 retroviral constructs, where the effects of Akt2 did not require IGF-1 (fig. S5).

To determine whether the miR-200 microRNA family also affects Akt activity, we transfected lung fibroblasts containing Akt1, Akt2, or Akt3 with miR-200a, miR-200c, or a control microRNA and measured the phosphorylation of all Akt isoforms before and 10 min after IGF-1 stimulation. We found that Akt phosphorylation was not affected by these microRNAs (fig. S6).

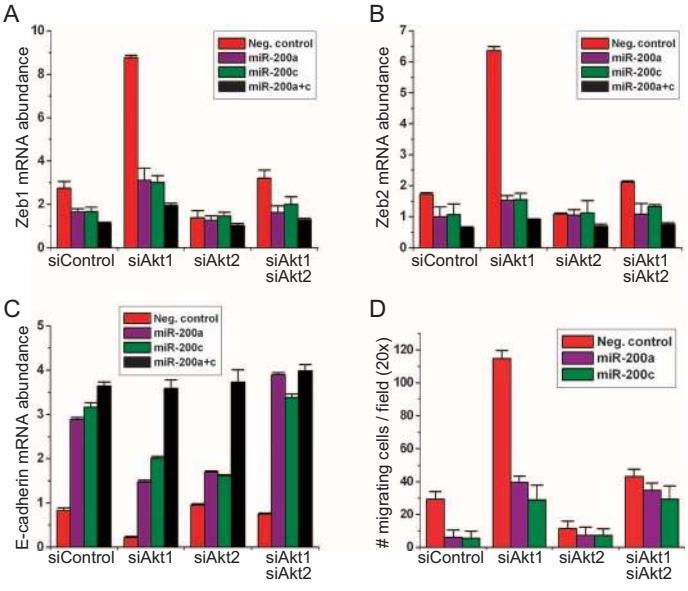

Fig. 4. Overexpression of miR-200a, miR-200c, and miR-200a plus miR-200c blocks the up-regulation of Zeb1 in MCF10A cells transfected with Akt1 siRNA and treated with TGFβ. (**A** and **B**) Overexpression of miR-200a or miR-200c inhibits the up-regulation of Zeb1 and Zeb2 in MCF10A cells transfected with Akt1 siRNA and treated with TGFβ. (**C**) Overexpression of miR-200a or miR-200c inhibits the down-regulation of E-cadherin in MCF10A cells transfected with Akt1 siRNA and treated with TGFβ. Abundance of the mRNAs encoding Zeb1, Zeb2, and E-cadherin was measured by real-time PCR in lysates of TGFβ-treated MCF10A cells transfected with the indicated siRNAs. (**D**) Overexpression of miR-200a or miR-200c inhibits cell migration in MCF10A cells transfected with Akt1 siRNA and treated with TGFβ. Cell migration was measured in TGFβ-stimulated MCF10A cells 24 hours after transfection with the indicated siRNAs. Experiments were performed in triplicate and data are presented as mean ± SD.

Akt1 knockdown, but not that of Akt2 or of Akt1 and Akt2, promotes EMT by decreasing the abundance of the miR-200 microRNA family

Previous studies had shown that the microRNAs of the miR-200 family target the 3′ untranslated region of the mRNAs encoding the helix-loop-helix transcription factors Zeb1 and Zeb2 and inhibit them postranscriptionally. Zeb1 and Zeb2 function as transcriptional repressors of E-cadherin (*14*, *15*). We therefore postulated that knockdown of Akt1, leaving Akt2 and Akt3 intact, may induce EMT in epithelial cells by decreasing the abundance of the miR-200 microRNA family. To address this hypothesis, we first examined the effects of Akt1 knockdown on the abundance of the mRNAs encoding Zeb1, Zeb2, and E-cadherin in the mammary epithelial cell line MCF10A. This cell line undergoes EMT after exposure to transforming growth factor β (TGFβ) (*16*), which activates Akt in both MCF10A cells and murine lung fibroblasts (fig. S7).

The mRNAs encoding Akt1 and Akt2, which are present in similar abundance in untransfected MCF10A cells (fig. S8), were respectively knocked down by transfection with small interfering RNA (siRNA) directed against Akt1 or Akt2. However, transfection of these siRNAs alone or in combination had no effect on the abundance of the mRNA encoding Akt3 (Fig. 3A). After transfection with these siRNAs, the cells were analyzed for the abundance of Zeb1, Zeb2, and E-cadherin before and 24 hours after treatment with TGFβ. The knockdown of Akt1, but not that of Akt2, synergized with TGFβ to increase the abundance of the mRNAs encoding Zeb1 and Zeb2 and decrease the abundance of E-cadherin at both the mRNA and the protein levels. Moreover, knocking down Akt2 together with Akt1 attenuated the effects of Akt1 knockdown on the abundance of Zeb1, Zeb2, and E-cadherin (Fig. 3, B and C, and fig. S9). EMT also promotes cell migration. We therefore used parallel cultures of similarly treated cells to measured cell migration by means of a Transwell cell migration assay. These experiments showed that TGFβ enhanced the migration of untransfected and Akt1 siRNA–transfected MCF10A cells by 7.7 and 22 times, respectively ($P = 0.00015$ compared to the control siRNA-transfected cells treated with TGFβ), and the migration of cells transfected with both Akt1 and Akt2 siRNAs by 3 times ($P =$

0.05 compared to the control siRNA-transfected cells treated with TGFβ) (Fig. 3C, lower panel). Cell migration therefore exhibited an inverse correlation with the abundance of E-cadherin in MCF10A cells, as expected. The knockdown of Akt1, but not that of Akt2 or of Akt1 plus Akt2, also enhanced migration in the absence of TGFβ in MCF10A cells ($P = 0.00046$) (Fig. 3C, lower panel) and in the breast cancer cell lines MCF-7 and BT474 (fig. S10).

The increase in the abundance of Zeb1 and Zeb2 in MCF10A cells in which Akt1 was knocked down may be due to a decrease in the abundance of the miR-200 microRNA family (Fig. 3D, upper panel, and fig. S11) (*14*, *15*). We indeed showed that both the knockdown of Akt1 and the TGFβ treatment decreased the abundance of this microRNA family and that, when combined, the knockdown of Akt1 and TGFβ acted synergistically to decrease the abundance of these microRNAs (Fig. 3D, lower panel, and fig. S12). To determine the specificity of the effects of Akt1 knockdown, MCF10A cells transfected with Akt1 siRNA were treated with TGFβ and monitored for 6 days after transfection. As the effects of the Akt1 siRNA waned and Akt1 mRNA returned to its pretransfection value, miR-200a, miR-200c, and the mRNAs encoding Zeb1, Zeb2, and E-cadherin also returned to their pretransfection values (Fig. 3E and fig. S13). The preceding data combined suggest that changes in the relative abundance of Akt1 and Akt2 that favor Akt2 promote down-regulation of the miR-200 microRNA family in both fibroblasts and epithelial cells.

Overexpression of miR-200a and miR-200c inhibits the effects of TGFβ and Akt1 knockdown on Zeb1, Zeb2, and E-cadherin abundance and on cell migration

To determine whether the decrease in the abundance of miR-200 microRNAs produced by TGFβ and by the knockdown of Akt1 could mediate the observed changes in the abundance of Zeb1, Zeb2, and E-cadherin, we transfected MCF10A cells with miR-200a, miR-200c, or both miR-200a and miR-200c and examined the abundance of Zeb1 and Zeb2 mRNA 24 hours later. We found that both microRNAs, alone or combined, decreased the abundance of the mRNAs encoding Zeb1 and Zeb2 in cells treated with either TGFβ alone or with TGFβ, in combina-

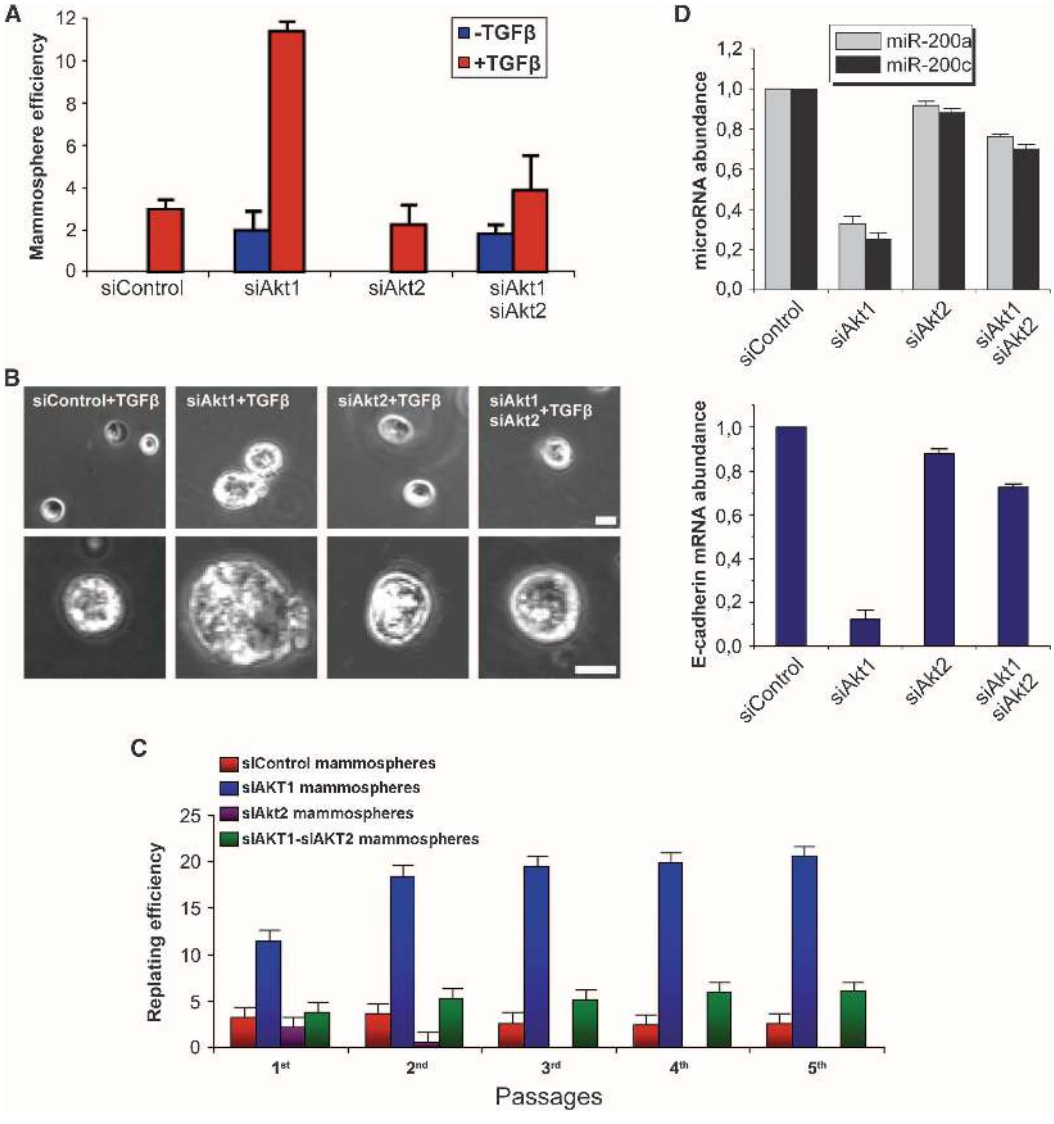

Fig. 5. Cells undergoing EMT through miR-200 down-regulation in response to TGFβ treatment and Akt1 knockdown exhibit stem cell properties. (**A**) MCF10A cells transfected with control siRNA or siRNAs for Akt1, Akt2, or Akt1 and Akt2 were cultured for 6 days in suspension in the presence or absence of recombinant TGFβ (20 ng/ml). The bar graph shows the number of mammospheres per 1000 plated cells in each culture (mean ± SD) at the end of the experiment. (**B**) Phase-contrast images (low and high magnification) of mammospheres described in (A). Scale bar, 100 μm. (**C**) Replating efficiency of mammospheres derived from MCF10A cultures transfected with siRNA control, and siRNAs for Akt1, Akt2, and Akt1 plus Akt2. (**D**) Primary mammospheres of MCF10A cells transfected with Akt1 siRNA have less miR-200a, miR-200c, and E-cadherin than do MCF10A cells transfected with control, Akt2, or Akt1 plus Akt2 siRNAs. MicroRNA and E-cadherin expression were measured in 6-day mammospheres by real-time RT-PCR. Experiments were performed in triplicate, and data are presented as mean ± SD.

tion with Akt1 siRNA (Fig. 4, A and B). MCF10A cells transfected with the combination of miR-200a and miR-200c failed to show a decrease in E-cadherin after treatment with TGFβ and Akt1 siRNA (Fig. 4C). Furthermore, transfection with miR-200a or miR-200c blocked the increase in migration produced by treatment with TGFβ and Akt1 siRNA (Fig. 4D). Together, these data indicate that Akt1 knockdown increases the abundance of Zeb1 and Zeb2 and promotes EMT by decreasing the abundance of the miR-200 microRNA family.

TGFβ- and Akt1 siRNA–treated cells undergoing EMT through a decrease in the abundance of miR-200 show a cancer stem cell–like phenotype

Metastases can arise when invasive cancer cells that travel to new sites act as tumor-initiating cells or cancer stem cells (*7*). We found that the knockdown of Akt1, but not that of Akt2, promoted formation of mammospheres—three-dimensional structures formed by breast cancer stem cells grown in suspension (*17*)—by MCF10A cells (Fig. 5B). Furthermore, Akt1 knockdown synergized with TGFβ in promoting mammosphere formation (Fig. 5, A and B). Akt1 and Akt2 knockdown in MCF10A cells did not affect the abundance of the mRNAs encoding the nontargeted isoforms and persisted for more than 6 days after siRNA transfection (fig. S14). Mammospheres in the Akt1 siRNA–treated cultures were larger than those in cultures treated with control siRNA; in addition, they showed higher replating potential and decreased abundance of miR-200a, miR-200c, and the mRNA encoding E-cadherin (Fig. 5, B to D). In the same mammospheres, the abundance of E-cadherin mRNA progressively decreased and the abundance of vimentin mRNA progressively increased over a 6-day period (fig. S15). Thus, Akt1 knockdown elicits a cancer stem cell–like phenotype, an observation consistent with the hypothesis that cells undergoing EMT acquire cancer stem cell properties (*18*). Thus, our data indicate that a decrease in miR-200 abundance after a shift in the balance between Akt1 and Akt2 promotes a cancer stem cell–like phenotype.

Mammary adenocarcinomas in MMTV-ErbB2/*Akt1*$^{-/-}$ mice have low abundance of all microRNAs of the miR-200 family, high abundance of Zeb1, and low abundance of E-cadherin

Expression of either ErbB2 or PyMT in the mammary gland of transgenic mice from mouse mammary tumor virus long terminal repeat (MMTV LTR)–driven transgenes causes mammary adenocarcinomas. Mammary adenocarcinomas that develop in MMTV-cErbB2/*Akt1*$^{-/-}$ mice were more invasive than those arising in MMTV-cErbB2/*Akt1*$^{+/+}$ mice, as determined by histological examination of the tumors; moreover, MMTV-cErbB2/*Akt1*$^{-/-}$ tumors may have a greater potential for metastasis (*5*). We confirmed the increased invasiveness of MMTV-cErbB2/*Akt1*$^{-/-}$ tumors compared to MMTV-cErbB2/*Akt1*$^{+/+}$ tumors (Fig. 6A) and found that ablation of Akt1 correlated with decreased abundance of the miR-200 microRNAs, as determined by real-time RT-PCR and in situ hybridization (Fig. 6, B and D, and fig. S16). Loss of Akt1 in these tumors was also associated with an increase in the abundance of Zeb1 and vimentin and a decrease in that of E-cadherin, as determined by Western analysis (Fig. 6C and fig. S17) and immunofluorescence (Fig. 6D).

The Akt–miR-200–E-cadherin axis contributes to the metastatic phenotype of human mammary adenocarcinomas

We used real-time RT-PCR to evaluate the abundance of miR-200a, miR-200c, and the mRNAs encoding Akt1, Akt2, and E-cadherin in primary and metastatic tumor tissue from eight patients with breast cancer. The ratio of Akt1 to Akt2 was lower in metastatic than in primary tumor tissue in all but two cases, in which this ratio was high in both the primary and the metastatic tissue. The abundance of miR-200a, miR-200c, and the mRNA encoding E-cadherin was significantly lower in the metastatic tumors (Fig. 7A). These data suggest that decreased abundance of the miR-200 microRNA family and of E-cadherin are common features of metastatic human breast cancer and that this decrease may be associated with a decrease in the ratio of Akt1 to Akt2. We plotted the values of Akt1/Akt2, miR-200a, miR-200c, and E-cadherin for all six metastatic tumors in which the Akt1/Akt2 ratio was low and found an excellent correlation between these values, which we confirmed by the Spearman

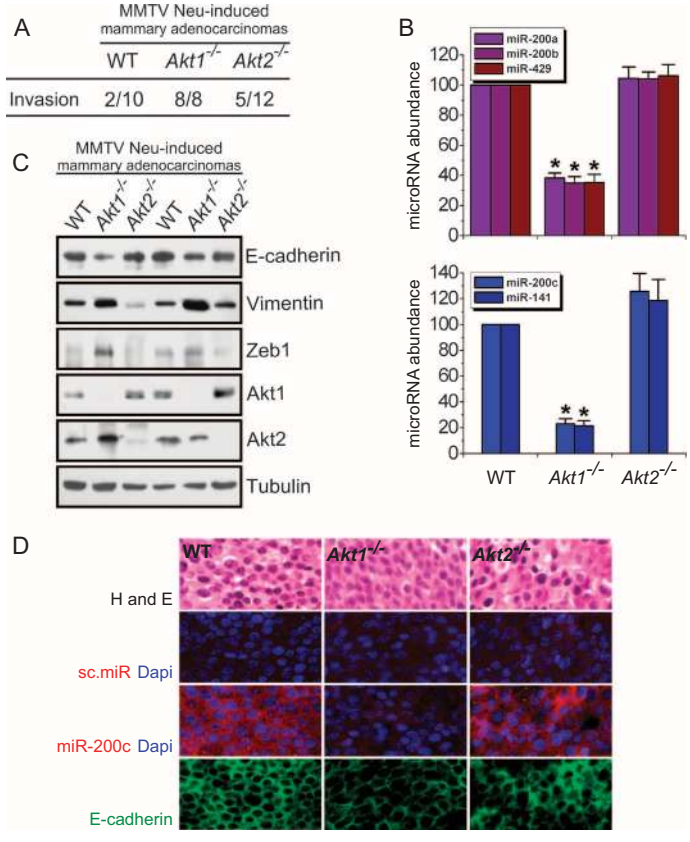

Fig. 6. Mammary adenocarcinomas developing in MMTV-cErbB2/*Akt1*$^{-/-}$ mice have low amounts of microRNAs of the miR-200 family, high amounts of Zeb1, and low amounts of E-cadherin. (**A**) Mammary adenocarcinomas developing in MMTV-cErbB2/*Akt1*$^{-/-}$ mice are more invasive than mammary adenocarcinomas arising in MMTV-cErbB2/WT and MMTV-cErbB2/*Akt2*$^{-/-}$ mice. (**B**) MMTV-cErbB2/*Akt1*$^{-/-}$ mammary adenocarcinomas have lower abundance of miR-200 microRNAs than do mammary adenocarcinomas developing in MMTV-cErbB2/*Akt1*$^{+/+}$ and MMTV-cErbB2/*Akt2*$^{-/-}$ mice. MicroRNA abundance was measured by real-time RT-PCR. (**C**) MMTV-cErbB2/*Akt1*$^{-/-}$ mammary adenocarcinomas have more abundant Zeb1 and vimentin and less abundant E-cadherin than do mammary adenocarcinomas developing in MMTV-cErbB2/*Akt1*$^{+/+}$ and MMTV-cErbB2/*Akt2*$^{-/-}$ mice. Western blots of primary tumor cell lysates were probed with the indicated antibodies. (**D**) In situ hybridization (for microRNA) and immunofluorescence (for E-cadherin) confirmed that MMTV-cErbB2/*Akt1*$^{-/-}$ mammary adenocarcinomas have low abundance of miR-200 family members and E-cadherin (microphotographs at 40× magnification). Scale bar, 10 μm.

rank correlation statistical test (Fig. 7B). These data suggest that breast cancer metastasis may frequently depend on signaling through the Akt–miR-200–E-cadherin axis. Given that the ratio of Akt1 to Akt2 was low in some primary tumors, it would be interesting to determine whether a low Akt1-to-Akt2 ratio has prognostic value for predicting metastasis.

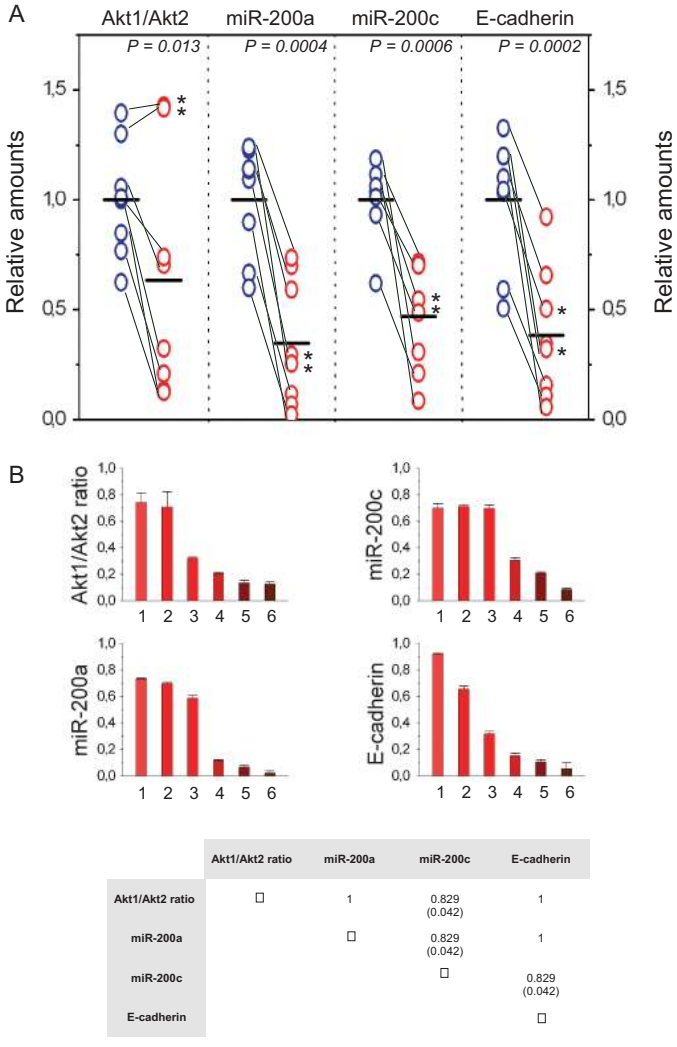

	Akt1/Akt2 ratio	miR-200a	miR-200c	E-cadherin
Akt1/Akt2 ratio	□	1	0.829 (0.042)	1
miR-200a		□	0.829 (0.042)	1
miR-200c			□	0.829 (0.042)
E-cadherin				□

Fig. 7. The Akt–miR-200–E-cadherin axis contributes to the metastatic phenotype in most human mammary adenocarcinomas. (A) The abundance of Akt1, Akt2, and E-cadherin mRNAs and microRNAs were measured by real-time RT-PCR in primary and metastatic tumors. The data represent triplicate measurements from each RNA sample normalized to GAPDH. Gray lines connect each primary tumor with the corresponding metastatic tumor. Asterisks are used to mark two cases in which the ratio of Akt1 to Akt2 remained high in the metastatic tumor sample despite the fact that miR-200 and E-cadherin abundances were lower than in the primary tumor samples from the same patients. The indicated *P* value ($P = 0.013$) was calculated with all tumors included. *P* values were calculated with a paired two-population Student's *t* test. The mean value for each set is shown as a horizontal black line. (B) Plotting the Akt1/Akt2 ratio and the expression of miR-200a, miR-200c, and E-cadherin in the six metastatic tumor samples characterized by low Akt1/Akt2 ratios [see (A)] revealed an excellent correlation between these parameters. Spearman rank correlation coefficients and the *P* values in parentheses are shown (lower panel).

DISCUSSION

Here, we show that after ablation of the floxed Akt1 allele, spontaneously immortalized $Akt1^{fl/fl}/Akt2^{-/-}/Akt3^{-/-}$ lung fibroblasts survived for about a week but failed to proliferate. Cells reconstituted with any of the three Akt isoforms survived and proliferated, suggesting that Akt1, Akt2, and Akt3 overlap functionally. However, comparison of cells reconstituted with Akt1, Akt2, or Akt3 also revealed functional differences. In this report, we present evidence for marked differences in microRNA signature between IGF-1– or TGFβ-treated cells expressing different Akt isoforms. In addition, we showed that the stimulation of cell migration induced by the knockdown of Akt1 but not Akt2 in cultured cells and the invasive phenotype induced by the ablation of Akt1 but not Akt2 in primary tumors are due to the differential effects of Akt1 and Akt2 on the abundance of the miR-200 microRNA family. These data suggest that the invasiveness and metastatic potential of human carcinomas may depend not on the expression and activity of Akt but on the balance between Akt1 and Akt2. A shift in the relative abundance or activity of Akt1 and Akt2 will alter the abundance of members of the miR-200 microRNA family and, consequently, the invasiveness and oncogenic potential of human tumors. Such a shift may occur naturally (*19*), or it may be elicited by Akt inhibitors that preferentially target Akt1 rather than Akt2. Our data suggest that we may be able to harness the beneficial effects of Akt1 inhibition, while prevent-

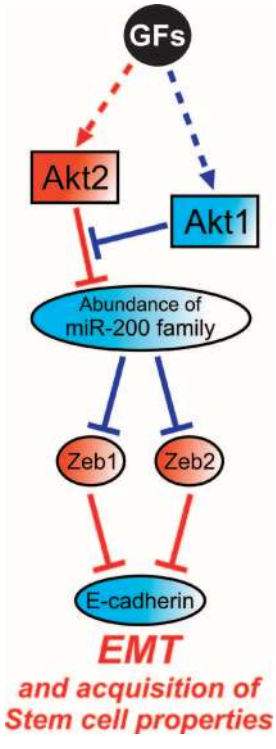

Fig. 8. Schematic diagram of the proposed model: The imbalance between Akt1 and Akt2 dysregulates microRNAs that control EMT and stem cell renewal programs. Red indicates a positive and blue indicates a negative role in the development of EMT. GFs, growth factors.

ing its unwanted effects on tumor cell invasiveness and metastasis, by combining Akt1 inhibition with delivery of microRNAs of the miR-200 microRNA family.

The regulation of the miR-200 microRNA family, through the concerted action of Akt1 and Akt2, appears to depend on the crosstalk between the two Akt isoforms (see model in Fig. 8). This model was based on the finding that Akt2, in the absence of Akt1, decreased the abundance of the miR-200 microRNA family and that Akt1 attenuated the Akt2-mediated decrease in the abundance of these microRNAs; however, Akt1 had no Akt2-independent effects on miR-200 family abundance. Based on these observations, we propose that Akt1 may regulate Akt2 or it may interfere with the Akt2-mediated decrease in miR-200 microRNA abundance downstream of Akt2. In either case, the role of Akt1 in miR-200 regulation appears to be Akt2 dependent.

Based on our current understanding of the biology of human cancer, Akt has been considered a high-priority therapeutic target (*20*). Pharmacological inhibitors for Akt, some of which are being evaluated in clinical trials (*21*, *22*), may differ with regard to their relative activities against Akt isoforms. Indeed, selective inhibition of Akt isoforms may be associated with lower toxicity (*23*). However, the data presented in this report suggest that preferential activity of a given compound against Akt1 or Akt2 may also have disadvantages. Given that tumors developing in the $Akt1^{-/-}$ genetic background grow slower than tumors developing in the wild-type and $Akt2^{-/-}$ genetic backgrounds, it is possible that an inhibitor that targets primarily Akt1 may cause cancer remission. However, if the tumor relapses, the tumor cells emerging after relapse may be significantly more aggressive, invasive, and metastatic. On the other hand, an inhibitor that targets primarily Akt2 may be ineffective. It is therefore important to test existing and future Akt inhibitors preclinically for potential differences in their ability to target Akt1, Akt2, and Akt3. Previous information regarding the sensitivity of the three Akt isoforms to a given inhibitor may allow us to design therapeutic strategies that maximize tumor responsiveness and prevent the unwanted selection of invasive and metastatic tumor cells. This report introduces a platform for the preclinical testing of the specificity of Akt inhibitors toward the three Akt isoforms.

In summary, the data presented here show that the balance between Akt1 and Akt2 is critical to the regulation of microRNA gene expression and that the opposing roles of Akt1 and Akt2 on the induction of EMT are due to the differential effects of the two Akt isoforms on the expression of the miR-200 microRNA family.

MATERIALS AND METHODS

Cell culture, constructs, and retroviral infections

Mouse lung fibroblasts from $Akt1^{fl/fl}/Akt2^{-/-}/Akt3^{-/-}$ mice were cultured in Dulbecco's modified Eagle's medium (DMEM) supplemented with 10% fetal bovine serum, penicillin and streptomycin, sodium pyruvate, nonessential amino acids, and glutamine. Passage of these cells every 3 to 4 days led to the establishment of spontaneously immortalized cell lines (*24*). Established cell lines were cultured in the same medium under standard culture conditions.

Wild-type Akt1, Akt2, and Akt3 tagged with the myc epitope at their C terminus were cloned in the retroviral vector pBabe-puro. Retrovirus constructs were packaged in 293T cells transiently transfected with these constructs and with an ecotropic virus Env construct. Immortalized lung fibroblasts were infected with the packaged viruses as follows: Cells were pretreated with DEAE-dextran (25 μg/ml). Forty-five minutes later, they were washed and infected. Infected cells were selected for puromycin (Sigma) resistance (2 μg/ml). Cells generated from three independent infections for each retroviral construct were analyzed for Akt by probing their lysates with antibodies against myc (#2276), Akt1 (#2938), Akt2 (#2964), and Akt3 (#3788, Cell Signalling Technologies). To abolish the expression of endogenous Akt1, cells were superinfected with a MigR1-GFP–based construct of the Cre recombinase and were sorted 48 hours later. To avoid puromycin selection, $Akt1^{fl/fl}/Akt2^{-/-}/Akt3^{-/-}$ lung fibroblasts were alternatively transduced with mycAkt1, mycAkt2, or mycAkt3 in the retroviral vector MigR1-GFP, and cells transduced with the respective viruses were superinfected with a MigR1-RFP (red fluorescent protein)–based construct of the Cre recombinase. Ablation of endogenous Akt1 by Cre gave rise to Akt-null cells [triple knockout (TKO)] or triple Akt knockout cells expressing a single Akt isoform at a time. In another set of experiments, we transduced the same lung fibroblast cell line with myrAkt1, myrAkt2, or myrAkt3 tagged with the hemagglutinin epitope.

To determine whether the effects of individual Akt isoforms on regulating miR-200 family also occurs in primary mouse embryo fibroblasts (MEFs), we carried out experiments using MEFs from wild-type, $Akt1^{fl/fl}/Akt2^{+/+}/Akt3^{-/-}$, $Akt1^{+/+}/Akt2^{-/-}/Akt3^{-/-}$, and $Akt1^{fl/fl}/Akt2^{-/-}/Akt3^{-/-}$ mice. To knock out the endogenous floxed Akt1 allele, we transduced with a MigR1-GFP-Cre construct.

MCF10A mammary epithelial cells were grown in DMEM/F12 medium supplemented with 5% donor horse serum, epidermal growth factor (EGF, 20 ng/ml), insulin (10 μg/ml), hydrocortisone (100 μg/ml), cholera toxin (1 ng/ml), and penicillin and streptomycin (50 U/ml).

Human breast cancer samples

RNAs from eight primary tumors and their corresponding metastatic tumors were purchased from Biochain Inc. These samples were used for real-time RT-PCR for E-cadherin, miR-200a, miR-200b, Akt1, and Akt2. Glyceraldehyde-3-phosphate dehydrogenase (GAPDH) expression levels were used as a loading control.

MicroRNA expression analysis

The abundance of 365 microRNAs was evaluated with TaqMan Low Density Arrays microRNA v1.0 arrays (Applied Biosystems). Cells were serum-starved overnight. Sixteen hours later, they were stimulated with IGF-1 (50 ng/ml) and were harvested 1, 4, and 16 hours later. Differentially expressed microRNAs were clustered with hierarchical clustering analysis. Changes in microRNA abundance were illustrated with heat maps. Blue color represents down-regulation, whereas red represents up-regulation of a given microRNA in IGF-1–treated fibroblasts.

MicroRNA real-time PCR analysis

Validation of microRNA array data was performed with the mirVana qRT-PCR miRNA Detection Kit and qRT-PCR Primer Sets according to the manufacturer's instructions (Ambion Inc). The expression of RNU48 and RNU44 was used as internal control. Real-time RT-PCR analysis was also performed to determine the abundance of miR-200a, miR-200b, miR-200c, miR-141, and miR-429 in MCF10A cells transfected with a negative control siRNA designed to have no sequence similarity to any human transcript sequence (#AM4611) or siRNAs against Akt1 (#S660), Akt2 (#S1216, Ambion Inc), or both and treated with TGFβ (20 ng/ml) for 24 hours. The abundance of these microRNAs was also normalized to RNU48 and RNU44 expression (internal controls). Data in Fig. 2, D and E, show the relative abundance of miR-200 family members at different time points after IGF-1 treatment. Their abundance before treatment was set at 0. Figure 3D shows the relative abundance of miR-200 family members in MCF10A cells treated with siRNAs directed against Akt1 or Akt2, and TGFβ. Here, microRNA abundance in cells transfected with the control siRNA and not treated with TGFβ was set at 1.

Real-time PCR analysis

Total RNA was extracted with Trizol (Invitrogen) according to the manufacturer's instructions. Complementary DNA (cDNA) was synthesized from 2.0 μg of total RNA by random priming with the Omniscript reverse transcription kit (Qiagen). Real-time PCR was performed in triplicate with the Quantitect SyBr green PCR system (Qiagen) on a Rotorgene 6000 series PCR machine (Corbett Research). All mRNA quantification data were normalized to β-actin, which was used as an internal control. The following primer sets were used: for Zeb1, 5′-TTCAAACCCATAGTGGTTGCT-3′ (forward) and 5′-TGGGAGATACCAAACCAACTG-3′ (reverse); for Zeb2, 5′-CAAGAGGCGCAAACAAGC-3′ (forward) and 5′-GGTTGGCAATACCGTCATCC-3′ (reverse); for E-cadherin, 5′-TGCCCAGAAAATGAAAAAGG-3′ (forward) and 5′-CTGGGGTATTGGGGGCATC-3′ (reverse); for vimentin, 5′-GAGAACTTTGCCGTTGAAGC-3′ (forward) and 5′-CTAACGGTGGATGTCCTTCG-3′ (reverse); and for Akt1/2, 5′-CTTCGAGCTCATCCTCATGG-3′ (forward) and 5′-TCTGCTTGGGGTCCTTCTTA-3′ (reverse).

Western blot analysis

Fibroblasts were lysed on ice with a Triton X-100 lysis buffer [50 mM tris (pH 7.5), 150 mM NaCl, 1 mM EDTA, 1mM EGTA, 1% Triton X-100, 2.5 mM sodium orthovanadate, 1 mM phenylmethylsulfonyl fluoride, 50 mM NaF, leupeptin (10 μg/ml), and aprotinin (5 μg/ml)]. Twenty micrograms of total protein from each sample was resolved in a 10% SDS-PAGE and transferred to polyvinylidene difluoride (PVDF) membranes. The blots were then probed with antibodies against phospho-Akt (Ser^{473} and Thr^{308}) (# 9271 and # 9275, Cell Signaling Technologies) and against tubulin (T5168, Sigma).

Transfected MCF10A cells were lysed on ice with an NP-40 lysis buffer [50 mM tris (pH 7.5), 150 mM NaCl, and 0.5% NP-40]. Fifty micrograms of total protein from each sample was resolved in a 4 to 12% bis-tris gel with Mops running buffer and transferred to PVDF membranes. The blots were then probed with antibodies against E-cadherin (610404, BD Biosciences) and β-actin (ab8227, Abcam Inc).

Transwell migration assay

Transwell migration assays were performed as described previously (*8*). Briefly, MCF10A cells were transfected with a negative control siRNA designed to have no sequence similarity to any human transcript sequence (#AM4611, Ambion) or siRNAs for Akt1 (#S660) or Akt2 (#S1216), or siRNAs for both Akt1 and Akt2 (50 nM). Twenty-four hours after transfection, they were cultured overnight in assay medium [MCF10A growth medium containing 2% serum ± TGFβ (20 ng/ml)]. Sixteen hours later, cells were trypsinized and 10^5 cells were added to the top chambers of 24-well Transwell plates (8-μm pore size; BD Biosciences). The bottom chambers were filled with assay medium. After overnight incubation, the migratory cells were fixed and stained with 0.1% crystal violet. The significance of variability between a given group and its corresponding control was determined with the unpaired *t* test.

Mammosphere culture

MCF10A cells were transfected with a control siRNA, siRNAs for Akt1 or Akt2, or siRNAs for both Akt1 and Akt2 (150 nM). Twenty-four hours later, cells were cultured in suspension in low-attachment plates (Corning) (1000 cells/ml) in serum-free DMEM/F12 medium supplemented with B27 (1:50, Invitrogen), 0.4% bovine serum albumin (BSA), EGF (20 ng/ml; Sigma), insulin (4 μg/ml; Sigma), and 1% methyl cellulose to prevent cell aggregation, in the presence or absence of TGFβ (20 ng/ml). Mammospheres with a diameter of >75 μm were counted 6 days later. To propagate mammospheres in vitro, mammospheres were collected by gentle centrifugation and dissociated to single cells as described (*17*). Before replating, mammosphere-derived cells were retransfected with 150 nM of the corresponding siRNAs (control, Akt1, Akt2, or both Akt1 and Akt2). Replating potential describes the ability of single cells to form mammospheres when cultured in new vessels.

Mouse experiments

The establishment of homozygous MMTV Neu transgenic mice in the wild type, $Akt1^{-/-}$, and $Akt2^{-/-}$ genetic backgrounds was previously described (*5*). Tissues were paraffin-embedded, sectioned, and stained with hematoxylin and eosin. Histologic sections were blindly analyzed. Invasive tumors were evidenced by infiltrative tumor foci in distinction from encapsulated tumor borders. The code was broken only when all the data were compiled.

Protein isolation and RNA isolation were performed with the mirVana PARIS Kit according to the manufacturer's instructions (Ambion). Protein extracts were analyzed by Western blot for E-cadherin (#3195, Cell Signaling Technologies), vimentin (sc-7558), and Zeb1 (sc-10572, Santa Cruz Biotechnology).

In situ microRNA hybridization

For in situ hybridization, MiRCURY LNA detection probes 3′-end-labeled with digoxigenin (DIG) for mmu-miR-200c (39549-05) or scramble-miR (99004-05, Exiqon) were used as previously described (*25*) with modifications. Sections (5 μm) of formalin-fixed paraffin-embedded Neu/wild-type, Neu/$Akt1^{-/-}$, and Neu/$Akt2^{-/-}$ tumors were deparaffinized in xylene, 2 × 40 min on a 50 rpm shaker, followed by 5 min each in serial dilutions of ethanol (100, 100, 75, 50, and 25%), followed by two changes of diethyl pyrocarbonate (DEPC)–double-distilled water (ddH_2O). Slides were then submerged for 5 min in 0.2 N HCl, washed with DEPC–phosphate-buffered saline (PBS), digested with proteinase K (40 μg/ml) for 20 min at 25°C, rinsed in 0.2% glycine/DEPC-PBS and 3× DEPC-PBS, and post-fixed with 4% formaldehyde in PBS for 10 min. Slides were then rinsed twice with DEPC-PBS, treated with acetylation buffer (300 μl of acetic anhydride, 670 μl of triethanolamine, 250 μl of 12 N HCl per 48 ml of ddH_2O) and then rinsed four times in DEPC-PBS followed by two rinses in 5 × SSC. Slides were prehybridized at 53°C for 2 hours in hybridization buffer [50% formamide, 5 × SSC, 0.1% Tween-20, adjusted to pH 6.0 with 9.2 mM citric acid, heparin (50 μg/ml), and yeast transfer RNA] in a humidified chamber (50% formamide, 5 × SSC). After prehybridization, slides were hybridized overnight at 53°C in a humidified chamber with 20 nM probe in prewarmed hybridization buffer. Sections were rinsed twice in 5 × SSC, followed by three washes of 20 min at 53°C in 50% formamide and 2 × SSC. Sections were then rinsed five times in PBS–0.1% Tween-20 (PBST), and blocked for 1 hour in blocking solution [2% sheep serum, BSA (2 mg/ml) in PBST]. Antibody against DIG-AP Fab fragments (11093274910, Roche) was applied on sections overnight at 4°C. Next, slides were washed two times in PBST for 10 min each and washed three times for 10 min each in 0.1 M tris-HCl (pH 7.5)/0.15 M NaCl, followed by equilibration with 1 M tris (pH 8.2) for 10 min and the Fast Red (Roche) solution [1 tablet per 2 ml of 0.1 M tris-HCl (pH 8.2)]. After incubation for 30 min in the dark, slides were washed three times in PBST for 10 min and coverslipped in Vectashield mounting medium with 4,6′-diamidino-2-phenylindole (DAPI; Vector Labs).

Sections of the tumors were deparaffinized in xylene, 3 × 5 min, followed by 10 min each in serial dilutions of ethanol (100, 100, 95, and 95%) and followed by two changes of ddH_2O. Antigen unmasking was achieved by boiling the slides (95°C to 99°C) for 10 min in 10 mM sodium citrate buffer (pH 6.0). Sections were then rinsed three times in ddH_2O and once in PBS and blocked for 1 hour in blocking solution (5% goat serum,

300 μl of Triton-X 100 in 100 ml of PBS). E-cadherin antibody was diluted (1:200) and applied on sections overnight at 4°C. Next, slides were washed three times in PBS for 5 min each and incubated with Cy2-conjugated antibody against goat immunoglobulin G diluted 1:500 for 1 hour at room temperature in the dark. Slides were washed three times in PBS for 5 min each and coverslipped in Vectashield mounting medium with DAPI.

Images were obtained with a Nikon Eclipse 80i microscope and a Spot charge-coupled device camera (Diagnostic Instruments). All photographs were processed using identical settings for capturing and further processing.

SUPPLEMENTARY MATERIALS

www.sciencesignaling.org/cgi/content/full/2/92/ra62/DC1

Fig. S1. Abundance of the three Akt isoforms in spontaneously immortalized lung fibroblasts transduced with retroviral constructs of Akt1, Akt2, or Akt3 and in primary lung fibroblasts from wild type mice.

Fig. S2. Heat map of differentially expressed microRNAs in untreated and IGF-1-treated fibroblasts, expressing no Akt (TKO), or individual Akt isoforms.

Fig. S3. Validation of microRNA microarray data by SYBR Green real-time RT-PCR analysis in Akt1-, Akt2-, and Akt3-expressing fibroblasts.

Fig. S4. Abundance of miR-200a and miR-200c in spontaneously immortalized lung fibroblasts from *Akt1*$^{fl/fl}$/*Akt2*$^{-/-}$/*Akt3*$^{-/-}$ mice transduced with MigR1-GFP constructs of Akt1, Akt2, or Akt3 and MigR1-RFP-Cre.

Fig. S5. Down-regulation of miR-200 microRNA family members in myrAkt2-expressing cells.

Fig. S6. Akt1, Akt2 and Akt3 phosphorylation by IGF-1 is not affected by overexpression of miR-200a, miR-200c, or miR-200a plus miR-200c.

Fig. S7. TGFβ treatment (20 ng/ml) induces Akt phosphorylation (at Ser^{473}) in MCF10A mammary epithelial cells and in murine lung fibroblasts expressing each of the three Akt isoforms.

Fig. S8. MCF10A cells have similar amounts of Akt1 and Akt2.

Fig. S9. Akt1 and Akt2 have opposing effects on the induction of EMT.

Fig. S10. The knockdown of Akt1 enhances cell motility, whereas the knockdown of Akt2 does not.

Fig. S11. Genomic localization of miR-200 family members. miR-200b, miR-200a and miR-429 map in a cluster on chromosome 1, and miR-200c and miR-141, map in a second cluster on chromosome 12.

Fig. S12. The knockdown of Akt1 decreases the abundance of all the members of the miR-200 microRNA family.

Fig. S13. The abundance of miR-200a, and the mRNAs encoding Zeb1, and Zeb2 in MCF10A cells transfected with Akt1 siRNA, returned to the pretransfection values as the effects of the Akt1 siRNA on Akt1 abundance wane.

Fig. S14. Expression of Akt1 and Akt2 in adherent and non-adherent MCF10A cells treated with siRNAs for Akt1 and/or Akt2 (harvested on the 6th day of culture at passage 5).

Fig. S15. E-cadherin and vimentin mRNA abundance in MCF10A cells, harvested at consecutive days of culture in suspension.

Fig. S16. MMTV-cErbB2-induced mammary adenocarcinomas express miR-200c and E-cadherin.

Fig. S17. MMTV-cErbB2/*Akt1*$^{-/-}$ mammary adenocarcinomas have more Zeb1 and vimentin and less E-cadherin than mammary adenocarcinomas developing in MMTV-cErbB2/*Akt1*$^{+/+}$ and MMTV-cErbB2/*Akt2*$^{-/-}$ mice.

Table S1. The microRNA signatures of immortalized lung fibroblasts expressing a single Akt isoform at a time and responding to IGF-1 differ.

Table S2. Comparison of the microRNA signatures of triple Akt knockout (TKO) lung fibroblasts, and their derivatives expressing Akt1, Akt2 or Akt3.

References

REFERENCES AND NOTES

1. A. Bellacosa, J. R. Testa, S. P. Staal, P. N. Tsichlis, A retroviral oncogene, akt, encoding a serine-threonine kinase containing an SH2-like region. *Science* **254**, 274–277 (1991).
2. T. F. Franke, S. I. Yang, T. O. Chan, K. Datta, A. Kazlauskas, D. K. Morrison, D. R. Kaplan, P. N. Tsichlis, The protein kinase encoded by the Akt proto-oncogene is a target of the PDGF-activated phosphatidylinositol 3-kinase. *Cell* **81**, 727–736 (1995).
3. B. D. Manning, L. C. Cantley, AKT/PKB signaling: Navigating downstream. *Cell* **129**, 1261–1274 (2007).
4. D. A. Altomare, J. R. Testa, Perturbations of the AKT signaling pathway in human cancer. *Oncogene* **24**, 7455–7464 (2005).
5. I. G. Maroulakou, W. Oemler, S. P. Naber, P. N. Tsichlis, Akt1 ablation inhibits, whereas Akt2 ablation accelerates, the development of mammary adenocarcinomas in mouse mammary tumor virus (MMTV)-ErbB2/neu and MMTV-polyoma middle T transgenic mice. *Cancer Res.* **67**, 167–177 (2007).
6. X. Ju, S. Katiyar, C. Wang, M. Liu, X. Jiao, S. Li, J. Zhou, J. Turner, M. P. Lisanti, R. G. Russell, S. C. Mueller, J. Ojeifo, W. S. Chen, N. Hay, R. G. Pestell, Akt1 governs breast cancer progression in vivo. *Proc. Natl. Acad. Sci. U.S.A.* **104**, 7438–7443 (2007).
7. A. C. Chiang, J. Massagué, Molecular basis of metastasis. *N. Engl. J. Med.* **359**, 2814–2823 (2008).
8. H. Y. Irie, R. V. Pearline, D. Grueneberg, M. Hsia, P. Ravichandran, N. Kothari, S. Natesan, J. S. Brugge, Distinct roles of Akt1 and Akt2 in regulating cell migration and epithelial-mesenchymal transition. *J. Cell Biol.* **171**, 1023–1034 (2005).
9. M. Yoeli-Lerner, G. K. Yiu, I. Rabinovitz, P. Erhardt, S. Jauliac, A. Toker, Akt blocks breast cancer cell motility and invasion through the transcription factor NFAT. *Mol. Cell* **20**, 539–550 (2005).
10. H. Liu, D. C. Radisky, C. M. Nelson, H. Zhang, J. E. Fata, R. A. Roth, M. J. Bissell, Mechanism of Akt1 inhibition of breast cancer cell invasion reveals a protumorigenic role for TSC2. *Proc. Natl. Acad. Sci. U.S.A.* **103**, 4134–4139 (2006).
11. G. A. Calin, C. G. Liu, C. Sevignani, M. Ferracin, N. Felli, C. D. Dumitru, M. Shimizu, A. Cimmino, S. Zupo, M. Dono, M. L. Dell'Aquila, H. Alder, L. Rassenti, T. J. Kipps, F. Bullrich, M. Negrini, C. M. Croce, MicroRNA profiling reveals distinct signatures in B cell chronic lymphocytic leukemias. *Proc. Natl. Acad. Sci. U.S.A.* **101**, 11755–11760 (2004).
12. J. Lu, G. Getz, E. A. Miska, E. Alvarez-Saavedra, J. Lamb, D. Peck, A. Sweet-Cordero, B. L. Ebert, R. H. Mak, A. A. Ferrando, J. R. Downing, T. Jacks, H. R. Horvitz, T. R. Golub, MicroRNA expression profiles classify human cancers. *Nature* **435**, 834–838 (2005).
13. C. M. Croce, Causes and consequences of microRNA dysregulation in cancer. *Nat. Rev. Genet.* **10**, 704–714 (2009).
14. P. A. Gregory, A. G. Bert, E. L. Paterson, S. C. Barry, A. Tsykin, G. Farshid, M. A. Vadas, Y. Khew-Goodall, G. J. Goodall, The miR-200 family and miR-205 regulate epithelial to mesenchymal transition by targeting ZEB1 and SIP1. *Nat. Cell Biol.* **10**, 593–601 (2008).
15. S. M. Park, A. B. Gaur, E. Lengyel, M. E. Peter, The miR-200 family determines the epithelial phenotype of cancer cells by targeting the E-cadherin repressors ZEB1 and ZEB2. *Genes Dev.* **22**, 894–907 (2008).
16. S. E. Seton-Rogers, Y. Lu, L. M. Hines, M. Koundinya, J. LaBaer, S. K. Muthuswamy, J. S. Brugge, Cooperation of the ErbB2 receptor and transforming growth factor β in induction of migration and invasion in mammary epithelial cells. *Proc. Natl. Acad. Sci. U.S.A.* **101**, 1257–1262 (2004).
17. G. Dontu, W. M. Abdallah, J. M. Foley, K. W. Jackson, M. F. Clarke, M. J. Kawamura, M. S. Wicha, In vitro propagation and transcriptional profiling of human mammary stem/progenitor cells. *Genes Dev.* **17**, 1253–1270 (2003).
18. S. A. Mani, W. Guo, M. J. Liao, E. N. Eaton, A. Ayyanan, A. Y. Zhou, M. Brooks, F. Reinhard, C. C. Zhang, M. Shipitsin, L. L. Campbell, K. Polyak, C. Brisken, J. Yang, R. A. Weinberg, The epithelial-mesenchymal transition generates cells with properties of stem cells. *Cell* **133**, 704–715 (2008).
19. S. Padmanabhan, A. Mukhopadhyay, S. D. Narasimhan, G. Tesz, M. P. Czech, H. A. Tissenbaum, A PP2A regulatory subunit regulates *C. elegans* insulin/IGF-1 signaling by modulating AKT-1 phosphorylation. *Cell* **136**, 939–951 (2009).
20. P. Dennis, in *American Association for Cancer Research Annual Meeting Education Book* (AACR, San Diego, CA, 2008), pp. 24–35.
21. G. Z. Cheng, S. Park, S. Shu, L. He, W. Kong, W. Zhang, Z. Yuan, L. H. Wang, J. Q. Cheng, Advances of AKT pathway in human oncogenesis and as a target for anti-cancer drug discovery. *Curr. Cancer Drug Targets* **8**, 2–6 (2008).
22. D. S. Levy, J. A. Kahana, R. Kumar, Akt inhibitor, GSK690693, induces growth inhibition and apoptosis in acute lymphoblastic leukemia cell lines. *Blood* **113**, 1723–1729 (2009).
23. C. Mao, E. G. Tili, M. Dose, M. C. Haks, S. E. Bear, I. Maroulakou, K. Horie, G. A. Gaitanaris, V. Fidanza, T. Ludwig, D. L. Wiest, F. Gounari, P. N. Tsichlis, Unequal contribution of Akt isoforms in the double-negative to double-positive thymocyte transition. *J. Immunol.* **178**, 5443–5453 (2007).
24. R. L. Meek, P. D. Bowman, C. W. Daniel, Establishment of mouse embryo cells in vitro. Relationship of DNA synthesis, senescence and malignant transformation. *Exp. Cell Res.* **107**, 277–284 (1977).
25. G. Obernosterer, J. Martinez, M. Alenius, Locked nucleic acid-based in situ detection of microRNAs in mouse tissue sections. *Nat. Protoc.* **2**, 1508–1514 (2007).

26. We thank N. Terrin for help with the statistical analyses and P. Hinds, C. Kuperwasser, and A. Charest of the Molecular Oncology Research Institute, Tufts Medical Center, for helpful discussions and for reviewing the manuscript. This work was supported by NIH grants NIH R01CA57436 (P.N.T) and R01CA107486 (K.S.) and a pilot project grant from the Tufts Medical Center Cancer Center (P.N.T). C.P. is a fellow of the Leukemia and Lymphoma Society.

Submitted 1 April 2009
Accepted 24 September 2009
Final Publication 13 October 2009
10.1126/scisignal.2000356

Citation: D. Iliopoulos, C. Polytarchou, M. Hatziapostolou, F. Kottakis, I. G. Maroulakou, K. Struhl, P. N. Tsichlis, MicroRNAs differentially regulated by Akt isoforms control EMT and stem cell renewal in cancer cells. *Sci. Signal.* **2**, ra62 (2009).